Propagation and Damping of Nonlinear Plasma Wave Packets

J. E. Fahlen*

Department of Electrical Engineering, University of California, Los Angeles, California 90095, USA

B. J. Winjum and T. Grismayer

Department of Physics and Astronomy, University of California, Los Angeles, California 90095, USA

W. B. Mori

*Department of Electrical Engineering, University of California, Los Angeles, California 90095
and Department of Physics and Astronomy, University of California, Los Angeles, California 90095, USA*
(Received 16 December 2008; published 17 June 2009)

Nonlinear electron plasma wave packets are shown to locally damp at the rear of the packet. Resonant particles enter the back of the packet and linearly damp the first few wavelengths, thereby carrying energy away from the back edge and eventually eroding the packet. This process could significantly affect the recurrence and long-time behavior of stimulated Raman scattering because it is predicted that a nonlinear packet will erode away before it travels a speckle length. The effects of a density gradient on the packet's propagation are also discussed.

The evolution of nonlinear plasma waves is a fundamental topic in basic plasma physics. This topic has received renewed attention due to its possible importance to laser-target coupling in laser-driven inertial confinement fusion (ICF). In ICF, stimulated Raman scattering (SRS) [1], in which the incident laser decays into a backscattered light wave and an electron plasma wave, can reflect the laser and hence reduce the coupling of laser energy to the target (see section III of [2], for example). In addition, the resulting plasma wave can trap electrons and lead to energetic electrons that can preheat the target. Recent fully kinetic SRS simulations with parameters relevant to ICF show SRS to be temporally bursty [3], with spatially localized plasma wave packets [4] that convect across the interaction region [5–7].

Nonlinear effects in infinite periodic waves have been studied in detail in [8–12], and much recent work has focused on plasma wave nonlinearities that affect SRS saturation [3–6,13,14]. There has also been recent work on dynamic long-lived nonlinear periodic trains [15]. Investigations on finite-length plasma wave packets, however, are not as extensive. Some authors have studied wave packets, but they focused on the dynamics of particles traversing a fixed amplitude wave packet, either numerically [16] or with adiabatic theory [17]. Many have also employed the Born approximation to estimate the linear damping rate [18,19] or energy distribution of scattered particles [20]. Others have combined theory and simulation to study the lengthening of packets due to detrapped particles [21], but without addressing the packet's energy loss. In this Letter, we show for the first time how a finite-length nonlinear plasma wave packet will erode away due to particle trapping. This is different from infinite periodic wave trains, which evolve into long-lived undamped BGK-like modes after several trapped-particle bounce times [10].

Plasma wave packets generally move at the wave's group velocity, $v_g = \partial \omega / \partial k = -\text{Re}[(\partial \epsilon / \partial k)/(\partial \epsilon / \partial \Omega)] = v_\phi + 2\sqrt{2} v_{\text{th}} \text{Re}[Z'(s)/Z''(s)]$, as this is the speed at which energy moves. Here, $s = \Omega / \sqrt{2} k v_{\text{th}}$, $Z(s)$ is the plasma dispersion function, $\Omega = \omega + i\gamma_L$ satisfies $\epsilon(\Omega, k) = 0$, and $v_\phi = \omega / k$ is the phase velocity. We will show in the following that the finite length of the packet combined with particle trapping effects leads to a faster apparent speed due to etching of the back of the wave packet.

Assume that, for this discussion, the wave packet envelope is a flat top many wavelengths long with a short rise and fall a few wavelengths long on either side. By "short" we mean the amplitude varies quickly enough that the adiabatic invariant J for the trapped particles is not constant. Such packets are often generated in kinetic simulations of SRS [4,5,7]. Figure 1 presents the electron phase-space from a sample particle-in-cell (PIC) simulation, described below, for such a packet, with (a) the rear and (b) the front of the packet at the same time. For the packets considered here, $v_\phi \gg v_g$, so particles with $v_\phi - v_T < v < v_\phi + v_T$ stream into the wave packet from behind and can become trapped, where $v_T = 2\sqrt{eE/mk}$ is the trapping width. Each wave period, since $v_\phi \gg v_g$, a new potential well emerges at the rear edge of the packet. Particles that enter at the appropriate velocity and phase will trap in this well. During approximately the first quarter of the bounce time ($\tau_B = 2\pi\sqrt{m/eEk}$) after the new well forms, the wave loses energy at approximately the linear Landau damping rate [10]. The linear Landau damping rate is appropriate, despite the large peak amplitude, because resonant electrons moving at approximately v_ϕ are only in the first few buckets for a fraction of a bounce time. Figure 1(a) depicts this process in the potential wells labeled "1" and "2," which are referred to as "buckets" in the following.
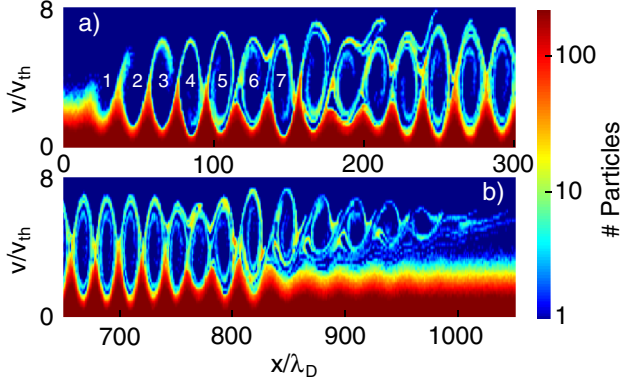
FIG. 1 (color online). Phase space for a packet with $k\lambda_D = 0.3$, peak amplitude of $eE/m\omega_p v_{\text{th}} \approx 0.55$, and length 30λ moving to the right at $t\omega_p = 135$. Plot (a) is the left side of the packet, plot (b) is the right. In (a), the newly trapped particles enter the rear of the packet. The sideband beat pattern begins to break up the phase-space vortices about 6 wavelengths into the packet. In b), detrapped particles stream forward ahead of the packet. The sidebands have not yet reached the front of the packet. The solid dark blue background represents no particles.

After $\tau_B/4$, the resonant particles begin to give their energy back to the wave as they ride up the far side of the potential well, as can be seen in bucket "3" in Fig. 1(a). The buckets, and hence the particles trapped in them, move at a speed of $v_\phi - v_g$ in the packet's frame, so that by the time the energy in each bucket begins to flow back to the wave, it has moved a distance $d_{\text{lin}} = \tau_B(v_\phi - v_g)/4$ into the packet. Each bucket effectively transports energy from the rearmost wavelength of the packet into the interior. The damping ceases as the trapped particles traverse the packet and phase mix [10], so only the rearmost part of the packet Landau damps. Each new phase front continues this process, allowing Landau damping to continually damp, or etch away, the wave energy at the rear of the packet. This model implicitly assumes that the packet length l is much larger than d_{lin}.

We will now estimate the etching rate, v_{etch}. As a wave Landau damps, it loses energy according to $dW/dt = -2\gamma_L W$, where W is the energy in a wavelength, $\frac{1}{8\pi}\lambda E^2 \text{Re}[\frac{\partial}{\partial\Omega}(\Omega\epsilon)]$, and $\text{Re}[\frac{\partial}{\partial\Omega}(\Omega\epsilon)] \approx 2$ describes the field and kinetic energy in a plasma wave. Each new bucket will Landau damp over a time $\tau_B/4$, and will therefore lose an amount $\Delta W_{\text{lost}} = \frac{1}{8\pi}\lambda E_0^2(1 - e^{-2\gamma_L\tau_B/4})\text{Re}[\frac{\partial}{\partial\Omega}(\Omega\epsilon)]$, where E_0 is the peak amplitude. In the wave frame, a new bucket forms in a time $\tau = \lambda/(v_\phi - v_g)$, so the rate of energy loss at the rear edge is $dW/dt = \Delta W_{\text{lost}}/\tau$. The etching rate can be calculated by finding the time Δt required to remove all the energy in a region Δx, $\frac{1}{8\pi}E_0^2\text{Re}[\frac{\partial}{\partial\Omega}(\Omega\epsilon)]\Delta x = (dW/dt)\Delta t$, giving

$$v_{\text{etch}} = \Delta x/\Delta t = (v_\phi - v_g)(1 - e^{-\gamma_L\tau_B/2}). \quad (1)$$

In the limit that $\gamma_L\tau_B \ll 1$, $v_{\text{etch}} = \gamma_L\tau_B(v_\phi - v_g)/2$. For long wavelength waves, $k\lambda_D \to 0$, no particles trap and the wave packet propagates essentially unchanged. As $k\lambda_D$

increases, v_{etch} becomes nonzero at $k\lambda_D \approx 0.2$ and the back of the wave erodes away more quickly. The etching rate increases sharply at low amplitude, since $\tau_B \propto 1/\sqrt{E_0}$, until the model breaks down when v_{etch} approaches v_ϕ.

To verify the simple model above, we performed numerous 1D electrostatic PIC simulations using the BEPS code over a range of wavelengths, from $k\lambda_D = 0.2$ to 0.4, each separated by 0.025. The simulations use 4096 cells and 8192 simulation particles per cell with a grid spacing of $\Delta_x = \lambda_D$ and a time step of $\Delta_t = 0.2\omega_p^{-1}$. Traveling waves with two different envelopes were excited using external drivers. The first has a flat-top envelope many wavelengths long and a short $1–2\lambda$ rise and fall, the second a symmetric envelope with the rise given by $10(x/L)^3 - 15(x/L)^4 + 6(x/L)^5$. In both cases, the driver is on for about two wave periods, and the spatial variations are such that the adiabatic conditions, $v_\phi\tau_B \ll 2\lambda$ for the flat top and $v_\phi\tau_B \ll L$ for the Gaussian-like pulse, are not satisfied. For each wave number, we varied the driver amplitude E_D by a factor of 100. For example, the waves driven at $k\lambda_D = 0.3$, shown in Fig. 2(c), have $eE_D/m\omega_p v_{\text{th}} = 0.002–0.2$, resulting in peak packet amplitudes between $eE/m\omega_p v_{\text{th}} \approx 0.0087–0.65$. In order for the etching model to be valid, the wave amplitude must be sufficiently large that $\gamma_L\tau_B < 1$. Otherwise, $v_\phi > v_{\text{etch}}$, or equivalently, the wave will damp in less than a bounce time. For each simulation, we chose an ω such that $\epsilon(\Omega, k) = 0$. For $k\lambda_D > 0.4$, the simple model appears to break down. For the simulation in Fig. 1, $k\lambda_D = 0.3$ and a flat-top spatial envelope 30λ long was used.

A comparison of the simulation results with the model shows excellent agreement with both the k and amplitude dependence. Figure 2(a) shows the etching rate as a function of $k\lambda_D$ for simulations with amplitudes of $eE/m\omega_p v_{\text{th}} = 0.09–0.16$. Figure 2(c) shows good agree-
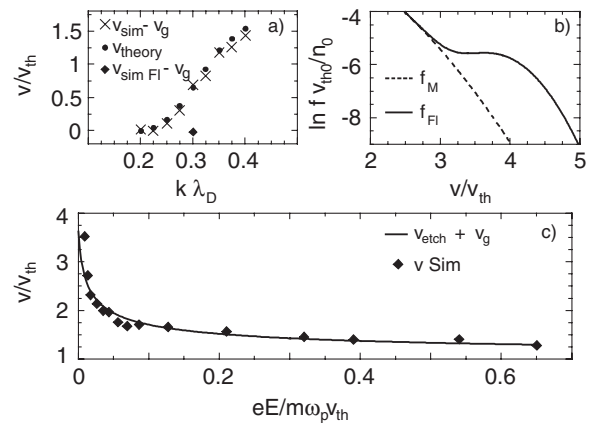

FIG. 2. (a) v vs $k\lambda_D$ with the rear-edge etching velocity measured from the simulations and calculated from the model for amplitudes near $eE/m\omega_p v_{\text{th}} = 0.1$, including the run using f_{Fl}. The calculations are made including the appropriate particle shape factor for the simulations. (b) Maxwellian and artificially flattened distribution function, with $n_1 = 0.004n_0$, $v_{\text{th1}} = 0.47v_{\text{th0}}$, $v_d = 3.77v_{\text{th0}}$. (c) v vs amplitude for $k\lambda_D = 0.3$.

ment between Eq. (1) and the simulations over a large range of amplitudes for $k\lambda_D = 0.3$. This choice of k allows etching velocity measurements over a wide range of amplitudes. The electric field for the smallest amplitude waves is actually below the noise in the simulations. For these cases, we use the subtraction technique [22], in which the fields from a run without the driver are subtracted from the same run with the driver so that the packet is clearly obtained. A comparison of the packet lifetime also gives reasonably good agreement with the simulations, as shown in Fig. 3(a). The model predicts that the wave will erode away completely by $\tau_{\text{etch}} = l/v_{\text{etch}} \approx 700\omega_p^{-1}$, which is in good agreement with the simulation. Figure 3(b) shows the same run with a periodic driver for comparison. In this simulation, the sideband instability breaks up the wave, but about 50% of the initial wave energy remains in the field at the end of the periodic simulation.

Wave packets also suffer sideband instabilities [6,12] that destroy the trapped-particle phase-space vortices traversing the packet but that do not affect the etching rate. Visible in Figs. 3(a) and 3(b) as striations propagating at approximately the group velocity, the sideband modulations allow trapped particles to stream from one bucket to the next. These result from the beating of the fundamental with the sideband modes. Figure 1(a) also shows this effect. In the wave packet case, the sequence of particle trapping usually considered in the temporal or initial value

(infinitely long) case is a sequence in space. Initially, we see in Fig. 1(a) that the wave Landau damps as the particles accelerate in buckets 1 and 2. Buckets 3 through 5 show the particles sloshing in their buckets as they phase mix (buckets 6 and after). Sidebands do not appear until bucket 6 or 7, where the distortion they cause to the potential wells of the wave allows some particles to stream into adjacent buckets. Thus, the etching process is not affected by sideband instabilities, since sideband growth requires the newly trapped particles to have bounced a few times. By this time, the bucket is several wavelengths into the packet, leaving the rear edge devoid of sidebands. At the time of the plot, the sidebands have not moved far enough into the packet to be visible at the right side of the packet [Fig. 1(b)]. Eventually, the sidebands lead to a complex interplay of trapped and detrapped particles in the central section of the packet, but the wave will still etch away in a time τ_p.

Ultimately, the trapped particles exit the packet at its front boundary, having traversed it at a speed near v_ϕ. These detrapped particles drive plasma waves in front of the packet at lower k, an effect that can be seen in Fig. 1(b) and in Fig. 3(a) to the right of the line labeled "v_g" [21]. We have reproduced some of the simulation results in [21], where short packets with $l \approx v_\phi\tau_B$ were studied. The trapped particles from short packets drive very well defined waves in front of the packet since they have not phase mixed and therefore exit the wave as a relatively coherent bunch. For the wave packets considered here, and for those observed in SRS simulations [3–7], phase mixing and sidebands disrupting the phase space cause a constant stream of particles to exit the packet. Consequently, the forward waves are not very well defined in our simulations, though we have observed them in nearly all the simulations we performed.

The appearance of linear Landau damping in Eq. (1) implies that the etching rate could be reduced by initializing the plasma with a flattened distribution function. Figure 2(b) shows a typical Maxwellian distribution (f_M) and an artificially flattened one $f_{\text{Fl}} = f_M + \frac{n_1}{\sqrt{2\pi}v_{\text{th1}}} \times e^{-(v-v_d)^2/v_{\text{th1}}^2}$. For a test case with $k\lambda_D = 0.3$, we find that for f_{Fl}, both the front and back of the packet move at nearly the same speed, in contrast to the strong etching case shown in Fig. 3(a). However, the linear group velocity with the flattening is about 60% higher than it would be without it, despite the second population accounting for only 0.4% of the total density. The front-edge velocity is actually slightly slower than the predicted group velocity in this case, so we use it instead for the data point in Fig. 2(a).

It is also of interest to consider the effects of a density gradient. For example, both SRS and the two plasmon decay instability [23] will excite plasma wave packets in a density gradient. Packets propagating in a gradient behave in much the same way as their homogeneous counterparts, except that k, v_ϕ, and v_g change with position. A change in the packet's behavior occurs, whether going up
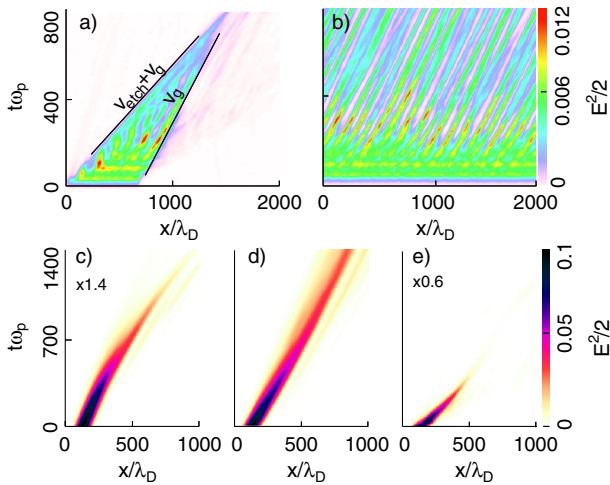

FIG. 3 (color online). Spatial and temporal average of the normalized electric field energy in units of $(e/m\omega_p v_{\text{th}})^2$. Plots (a) and (b) are from a uniform plasma simulation with a driver having $k\lambda_D = 0.325$ and amplitude $eE_D/m\omega_p v_{\text{th}} = 0.01$ lasting for $t\omega_p = 50$: (a) has a finite-length driver (30λ) with a flat top, while (b) has an infinitely long driver. At $t\omega_p = 800$, the wave in (a) has little energy left, while the infinite wave in (b) still has nearly 50% of its initial energy. Plots (c)–(e) show results for a Gaussian driver (FWHM = $4\lambda_0$, $eE_D/m\omega_p v_{\text{th}} = 0.06$, duration $t\omega_p = 15$). In (c), a wave with $k_i\lambda_D = 0.2$ accelerates down a density gradient of $\alpha = -1.95 \times 10^{-4}/\lambda_D$, while in (d) and (e), the wave has $k\lambda_D = 0.2$ and 0.26, respectively, and the density is constant. At $t\omega_p \approx 700$, the wave in (c) has $k\lambda_D \approx 0.26$.

or down a gradient, when $v_{\text{etch}}(k)$ first becomes significant, which we define as occurring at $k^\star \lambda_D \approx 0.2$. A packet moving through the gradient will reach a point where $k > k^\star$ and etch away regardless of its initial $k = k_i$ and direction. If $k_i < k^\star$ and the packet is moving down the gradient, it will eventually reach a location for which $k > k^\star$ and then etch away, with the process accelerating as the packet moves down the gradient. If it is initially moving up the gradient and $k_i < k^\star$, the packet will eventually reflect and begin to etch away as it moves down when $k > k^\star$. If $k_i > k^\star$, the packet may completely erode away before $k < k^\star$, or it may only partially etch before reflecting and continuing to etch away as it moves down the gradient.

Figure 3(c) shows a short packet propagating down a relatively steep density gradient. A slight curving is apparent due to the increase of v_g as the packet accelerates down the gradient. Initialized with $k\lambda_D = 0.2$, this packet is just about to begin to erode. By $t = 700\omega_p^{-1}$, the packet's wave number has increased to $k\lambda_D \approx 0.26$, leading to an increase in v_{etch}. We compare this behavior with the cases shown in Fig. 3(d) and 3(e). For these two cases, no gradient was used, but the waves were initialized with $k_i\lambda_D = 0.2$ (d) and $k_i\lambda_D = 0.26$ (e) in order to correspond with the wave's k in the density gradient case at $t = 0$ and $t = 700\omega_p^{-1}$, respectively. With $k\lambda_D = 0.2$, little etching occurs, allowing the packet to propagate for a relatively long time, while for $k\lambda_D = 0.26$, the packet rapidly etches away.

In SRS, as the instability saturates, plasma wave packets propagate forward and etch away, though the continuous presence of the driving laser and scattered light complicates the dynamics. However, etching still occurs as can be seen in, for example, Fig. 5 of Ref. [5]. To see that etching might be important for SRS at NIF-like conditions, consider an $f/4.5$ to $f/8$ beam that will give a speckle length of 4500 to $15\,000\lambda_D$ for $3\omega_0$ light. A typical packet 100λ long with $k\lambda_D = 0.3$ will take about 6000 to $19\,000\omega_p^{-1}$ to cross a speckle, while $\tau_p \approx 2000\omega_p^{-1}$. SRS driven plasma waves tend to be of relatively large amplitude ([7], for example), where the etching rate's amplitude dependence is weak, so we simply use $eE/m\omega_p v_{th} = 0.15$ for the calculation. Barring other effects, the packet will completely etch away long before it can cross the speckle. In NIF-like experiments, the interaction between multiple speckles could flatten the distribution function in some regions and cause the Landau damping and etching rates to vary. Accordingly, some packets may not etch at all, depending on the details of SRS in their surroundings, but mesoscale models of SRS should account for the possibility of etching.

We have demonstrated that in one dimension, finite-length nonlinear plasma wave packets with $k\lambda_D \gtrsim 0.2$ etch away at a rate given in Eq. (1). We estimate that this effect could destroy an SRS wave packet before it can traverse a speckle, though non-Maxwellian distributions due to multispeckle interactions could reduce or eliminate etching. Sidebands occur in wave packets with trapped particles, just as they do in infinite periodic plasma waves, but they do not quench the etching. The effects of a density gradient were also discussed.

*jfahlen@ucla.edu
[1] D. W. Forslund, J. M. Kindel, and E. L. Lindman, Phys. Fluids **18**, 1002 (1975).
[2] J. D. Lindl et al., Phys. Plasmas **11**, 339 (2004).
[3] H. X. Vu, D. F. DuBois, and B. Bezzerides, Phys. Rev. Lett. **86**, 4306 (2001); Phys. Plasmas **9**, 1745 (2002).
[4] L. Yin et al., Phys. Plasmas **13**, 072701 (2006).
[5] D. J. Strozzi, E. A. Williams, A. B. Langdon, and A. Bers, Phys. Plasmas **14**, 013104 (2007).
[6] S. Brunner and E. J. Valeo, Phys. Rev. Lett. **93**, 145003 (2004).
[7] B. J. Winjum et al., Bull. Am. Phys. Soc. **53**, 232 (2008).
[8] I. B. Bernstein, J. M. Greene, and M. D. Kruskal, Phys. Rev. **108**, 546 (1957).
[9] J. M. Dawson and R. Shanny, Phys. Fluids **11**, 1506 (1968).
[10] G. J. Morales and T. M. O'Neil, Phys. Rev. Lett. **28**, 417 (1972).
[11] E. Asseo, G. Laval, R. Pellat, R. Welti, and A. Roux, J. Plasma Phys. **8**, 341 (1972).
[12] W. L. Kruer, J. M. Dawson, and R. N. Sudan, Phys. Rev. Lett. **23**, 838 (1969).
[13] D. Benisti and L. Gremillet, Phys. Plasmas **14**, 042304 (2007); D. Bénisti, D. J. Strozzi, and L. Gremillet, Phys. Plasmas **15**, 030701 (2008).
[14] R. R. Lindberg, A. E. Charman, and J. S. Wurtele, Phys. Plasmas **14**, 122103 (2007).
[15] B. Afeyan et al. (private communication).
[16] V. Fuchs, V. Krapchev, A. Ram, and A. Bers, Physica (Amsterdam) **14D**, 141 (1985).
[17] D. L. Bruhwiler and J. R. Cary, Phys. Rev. Lett. **68**, 255 (1992); Phys. Rev. E **50**, 3949 (1994).
[18] O. Skjaeraasen, P. A. Robinson, and A. Melatos, Phys. Plasmas **6**, 3435 (1999).
[19] R. W. Short and A. Simon, Phys. Plasmas **5**, 4124 (1998).
[20] G. J. Morales and Y. C. Lee, Phys. Rev. Lett. **33**, 1534 (1974).
[21] J. Denavit and R. N. Sudan, Phys. Rev. Lett. **28**, 404 (1972).
[22] V. K. Decyk, Invited Paper at International Conference on Plasma Physics, Kiev, USSR, (World Scientific Publishing Company, Singapore, 1987).
[23] B. B. Afeyan and E. A. Williams, Phys. Rev. Lett. **75**, 4218 (1995), and references therein; A. B. Langdon, B. F. Lasinski, and W. L. Kruer, Phys. Rev. Lett. **43**, 133 (1979).